The impact of attenuation on the resolution of multicomponent seismic data

Richard A. Bale and Robert R. Stewart

ABSTRACT

In this paper, we undertake a comparative analysis of the expected effect of constant Q absorption on different modes, illustrating these effects by modelling absorption for homogeneous and layered models. We find that when S- and P-wave attenuation filters are compared in depth, they are exactly equal for the same Q value, in the homogeneous case. Higher wavenumbers for given frequencies in the source wavelet give an initial advantage to S-wave resolution in depth, which may be lost to attenuation if S-wave Q is less than P-wave Q, and/or if there are very low shear velocities in the near surface. Finally, dispersion, which inevitably accompanies attenuation, will differ for P and S modes with different Q values, resulting in event correlation errors. One, perhaps surprising, implication of this work is the need for better low-frequency recording to enhance shear-wave resolution. Additionally we provide relationships between interval and effective parameters including a Dix type inversion formula which could be used to derive shear-wave Q values from converted wave data.

INTRODUCTION

An important practical question for multicomponent seismic surveys is how absorption impacts shear or converted-wave resolution compared with that of P-waves. Converted-waves (specifically, those converting from P to S upon reflection) have the potential for providing higher resolution than P-waves, due to the shorter wavelengths associated with the same temporal frequencies. In practice, it is often observed that converted-wave resolution does not reach this ideal, particularly at depth. One possible reason suggested for this is the stronger effect of Q attenuation upon converted-waves. When considering the effect of absorption on converted-waves, we must consider two different values Q_P and Q_S, in much the same way as a medium has two different velocities V_P and V_S.

Rock physics provides a theoretical relationship, derived from complex elastic moduli, connecting the P-wave, S-wave, and bulk compressional Q values, Q_P, Q_S, and Q_K, as follows (e.g. Winkler and Nur, 1979):

$$\frac{1}{Q_P} = \frac{4}{3}\left(\frac{V_S}{V_P}\right)^2 \frac{1}{Q_S} + \left[1 - \frac{4}{3}\left(\frac{V_S}{V_P}\right)^2\right]\frac{1}{Q_K}$$

From this equation, and assuming an infinite value for Q_K, Udias (1999) argues that Q_S can be expected to be 4/9 of Q_P (if $V_P = \sqrt{3}V_S$). Whilst this is theoretically true for a dry medium, Winkler and Nur (1979) showed that for saturated or partially saturated media, one could equally find $Q_K \le Q_P$, in which case we would have $Q_S \ge Q_P$.

For a homogeneous medium, in the case where $Q_S > Q_P$, the PS resolution is expected always to exceed that of PP. Deffenbaugh et al. (2000) considered the case of a homogeneous medium with Q_S lower than Q_P, assuming a zero-phase Q response. They concluded that, in this case, there is a "crossover" point of equal PP and PS resolution, with the PS resolution surpassing that of PP above the crossover, but becoming poorer than PP below it. Our modelling confirms that Deffenbaugh et al.'s result holds true when minimum-phase dispersion is included.

The homogeneous case with $Q_S=Q_P$ was also considered recently by Garotta and Granger (2001). Their analysis is consistent with this paper, but also considers the important issues of amplitude differences between PP and PS modes, and signal to noise. For example, in the case where the average PS amplitude is half that of PP, with the same noise level, they note that attenuation can have a larger impact on shear wave resolution at depth, because the amount of signal above the noise floor is lower.

In this paper, we also consider the case where the medium is vertically inhomogeneous, with a variable V_P/V_S ratio. Our results indicate that velocity plays a rôle of equal importance to resolution as that of Q.

THEORY

A widely used model of seismic attenuation in the earth assumes a Q value that depends upon the medium, but not upon frequency – within the bandwidth of interest. This is known as the "constant Q model" of absorption, and a significant body of theory has been developed based upon it (e.g., Kjartannsen, 1979). Based on this assumption, a differential equation for the amplitude attenuation law can be obtained, which has the following solution:

$$A(x) = A_0 \exp\left(-|\omega| x / 2Qc\right) , \qquad (1)$$

where A_0 is the initial amplitude of a harmonic wave of frequency ω, and $A(x)$ is the amplitude after propagation by a distance x at velocity c, through a medium with a constant quality factor Q.

The application of equation (1) to a propagating pulse gives rise to a pulse that broadens symmetrically about a central peak. This situation entails a violation of causality, since some energy arrives before it has had the time to physically propagate. In a classic paper, Futterman (1962) showed, based on a causality argument, that there must inevitably be dispersion (velocity dependence on frequency) accompanying attenuation. He derived the attenuation-dispersion relationship when Q is constant over a wide range of frequencies. The resulting revised law of attenuation (see Appendix A) is given by the following equation:

$$A(x) = A_0 \exp\left(-\alpha(\omega)x + i\,\mathrm{H}[\alpha(\omega)]x\right) \qquad (2)$$

where H is the Hilbert transform, with respect to ω, and $\alpha(\omega) \equiv \dfrac{|\omega|}{2Qc}$.

Equation (2) may be recast in the time domain as follows:

$$A(t) = A_0 \exp\left(-\frac{|\omega|}{2Q} t + i\,\mathrm{H}\left(\frac{|\omega|}{2Q} \right) t \right) \tag{3}$$

Equation (2) may also be transformed to consider attenuation as a function of distance, x, and wavenumber, $k = \omega / c$:

$$A(z) = A_0 \exp\left(-\frac{|k|}{2Q} x + i\,\mathrm{H}\left(\frac{|k|}{2Q} \right) x \right) \tag{4}$$

Placing equation (2) within the context of a propagating pulse, with an initial spectrum $u(0,\omega)$ at $x = 0$, the pulse at a distance x, is $u(x,t)$, given by the following inverse Fourier transform:

$$u(x,t) = \frac{1}{2\pi} \int_{-\infty}^{\infty} u(0,\omega) \exp\left(i\omega\left(x/c - t \right) + i\,\mathrm{H}\left[\alpha(\omega) \right] x \right) e^{-\alpha(\omega) x} d\omega, \tag{5}$$

where c is the limiting velocity of the wave at the maximum frequency.

Q filters for pure and converted modes

We now derive the two-way Q-filter for PP, PS and SS waves, where in general $Q_S \neq Q_P$. Consider, for simplicity, the case of a single homogeneous layer with velocities V_P, V_S, and Q values Q_P, Q_S for the P and S waves respectively (Appendix B considers the more general, layered media, case). Expressed in the frequency domain, the PP Q-filter is simply the product of the one-way filter for P-waves with itself:

$$F_{PP}(z,\omega) = \exp\left(\frac{2i\omega}{V_P} z + 2i\,\mathrm{H}[\alpha_P(\omega)] z \right) \exp\left(-2\alpha_P(\omega) z \right), \tag{6}$$

noting that we replace x by z, since we consider propagation in the vertical direction only.

Similarly, the SS Q-filter is given by:

$$F_{SS}(z,\omega) = \exp\left(\frac{2i\omega}{V_S} z + 2i\,\mathrm{H}[\alpha_S(\omega)] z \right) \exp\left(-2\alpha_S(\omega) z \right), \tag{7}$$

and finally the PS (or SP) Q-filter is obtained by multiplying a 1-way P-wave filter by a 1-way S-wave filter:

$$F_{PS}(z,\omega) = \exp\left(\frac{i\omega}{V_P}z + i\,\mathrm{H}[\alpha_P(\omega)]z + \frac{i\omega}{V_S}z + i\,\mathrm{H}[\alpha_S(\omega)]z\right)\exp(-[\alpha_P(\omega)+\alpha_S(\omega)]z). \tag{8}$$

Equation (8) can be expressed in the following form:

$$F_{PS}(z,\omega) = \exp\left(\frac{2i\omega}{V_{PS}}z + 2i\,\mathrm{H}[\alpha_{PS}(\omega)]z\right)\exp(-2\alpha_{PS}(\omega)z), \tag{9}$$

by exploiting the linearity of the Hilbert transform, H, and making the following definitions:

$$\alpha_{PS} \equiv \frac{1}{2}(\alpha_P + \alpha_S) = \frac{|\omega|}{2Q_{PS}V_{PS}}, \tag{10}$$

$$\frac{1}{V_{PS}} = \frac{1}{2}\left(\frac{1}{V_P} + \frac{1}{V_P}\right), \tag{11}$$

and

$$\frac{1}{Q_{PS}} = \frac{V_{PS}}{2}\left(\frac{1}{Q_P V_P} + \frac{1}{Q_S V_S}\right). \tag{12}$$

As before, the Q filters described by equations (6) and (9) can be expressed in terms of two-way time, setting $T_{PP} = 2z/V_P$, and $T_{PS} = 2z/V_{PS} = z/V_P + z/V_S$ to give:

$$F_{PP}(T_{PP},\omega) = \exp\left(i\omega T_{PP} + i\,\mathrm{H}\left[\frac{|\omega|}{2Q_P}\right]T_{PP}\right)\exp\left(-\frac{|\omega|T_{PP}}{2Q_P}\right), \tag{13}$$

and

$$F_{PS}(T_{PS},\omega) = \exp\left(i\omega T_{PS} + i\,\mathrm{H}\left[\frac{|\omega|}{2Q_{PS}}\right]T_{PS}\right)\exp\left(-\frac{|\omega|T_{PS}}{2Q_{PS}}\right). \tag{14}$$

Comparison of equations (13) and (14) readily shows, in the case $Q_S=Q_P=Q$ (which also implies $Q_{PS}=Q_P$), that for any given depth of propagation and temporal frequency, ω, the S-wave attenuation is stronger than the P-wave attenuation, because $T_{PS}>T_{PP}$, for a given depth. This is intuitively sensible, since the slower shear velocity implies that the wave uses more cycles propagating from any given depth as an S-wave than as a P-wave. But this conclusion is unduly pessimistic for the following reason: ultimately, for the interpreter, the important criterion is the ability to resolve strata in depth, not in time. When interpreting time sections, the time scale of the PS events must be compressed to compare with P-wave events. Whether or not the data are transformed explicitly from time to depth, we must compare PP and PS resolution based on a common vertical coordinate. The resolution difference in the temporal frequency domain is compensated by the compression of the PS time scale required to compare it with PP time.

It is therefore convenient to consider attenuation as a function of depth and the real (undispersed) part of the wavenumber, $k = \omega / c$, giving:

$$F_{PP}(z, k_{PP}) = \exp\left(ik_{PP} z + i\,\mathrm{H}\left[\frac{|k_{PP}|}{2Q_P} \right] z \right) \exp\left(-\frac{|k_{PP}| z}{2Q_P} \right), \tag{15}$$

$$F_{PS}(z, k_{PS}) = \exp\left(ik_{PS} z + i\,\mathrm{H}\left[\frac{|k_{PS}|}{2Q_{PS}} \right] z \right) \exp\left(-\frac{|k_{PS}| z}{2Q_{PS}} \right), \tag{16}$$

where

$$k_{PP} \equiv \omega / V_P \text{ and } k_{PS} \equiv \omega / V_{PS}\,. \tag{17}$$

It is worth pointing out that these wave-numbers differ slightly from the true wave-numbers, which include dispersion. However, we shall assume that when the PP or PS traces are transformed to depth for comparison, the resulting wave-numbers are those given by (17). In other words the depth mapping corresponds to the limiting phase velocity at ω_∞.

In the homogeneous case, comparing P and S filter responses for the *same* wavenumber (necessarily corresponding to *different* temporal frequencies), we see that in the case that Q_S=Q_P=Q, the predicted attenuations are the same. To see why this is so, recall that the number of cycles executed for a particular wavelength is given by distance travelled divided by wavelength, and does not depend upon the velocity.

Layered Media

In the case of a layered medium and considering the simplest case of vertical wave propagation (hence using z instead of x for distance), the Q filters may be combined recursively for each layer (see Appendix B). The result is that equation (2) holds true where Q is replaced by an "effective Q" value, Q_{eff}, given by:

$$T/Q_{eff} = \sum_{n=1}^{N} \Delta z_n / Q_n c_n\,, \tag{18}$$

where

$$T \equiv \sum_{n=1}^{N} \Delta z_n / c_n\,.$$

Here $\Delta z_n \equiv z_n - z_{n-1}$ is the thickness of layer n, c_n is the velocity, and Q_n the Q value, in layer n. T is the total one-way travel time. An integral expression for effective Q, equivalent to (4), is given in Bickel and Natarajan (1985).

As shown in Appendix B, a similar approach, leads to an expression for the PS effective Q, $Q_{PS,eff}$, in terms of the effective Q values for P and S, $Q_{P,eff}$ and $Q_{S,eff}$:

$$\frac{T_{PS}}{Q_{PS,eff}} = \frac{T_P}{Q_{P,eff}} + \frac{T_S}{Q_{S,eff}}, \qquad (19)$$

$$T_{PS} \equiv T_P + T_S ,$$

where T_P and T_S here are one-way P and S times. Alternatively, the effective Q for PS data can be given in terms of average vertical P and S-wave velocities, V_P and V_S, as follows:

$$\frac{1}{Q_{PS,eff}} = \frac{V_{PS}}{2}\left(\frac{1}{Q_{P,eff}V_P} + \frac{1}{Q_{S,eff}V_S}\right), \qquad (20)$$

where

$$\frac{1}{V_{PS}} = \frac{1}{2}\left(\frac{1}{V_P} + \frac{1}{V_P}\right),$$

and V_{PS} is the usual definition of average PS velocity, which relates vertical two-way time to depth for a PS wave, and governs post-stack migration (Harrison and Stewart, 1993).

In Appendix B we also derive a Dix-type inversion for interval Q_S:

$$\frac{1}{Q_{S,N}} = \frac{v_{S,N}}{z_N}\left(\frac{T_{PS}^{(N)}}{Q_{PS,eff}^{(N)}} - \frac{T_{PS}^{(N-1)}}{Q_{PS,eff}^{(N-1)}}\right) - \frac{v_{S,N}}{Q_{P,N}v_{P,N}}$$

$$= \frac{1}{t_{S,N}}\left(\frac{T_{PS}^{(N)}}{Q_{PS,eff}^{(N)}} - \frac{T_{PS}^{(N-1)}}{Q_{PS,eff}^{(N-1)}}\right) - \frac{1}{Q_{P,N}\gamma} \qquad (21)$$

where $\gamma_N = v_{P,N}/v_{S,N}$ and the one-way shear interval time $t_{S,N}$ may be obtained from:

$$t_{S,N} = \frac{T_{PS}^{(N)} - T_{PS}^{(N-1)}}{1 + 1/\gamma}$$

and $Q_{P,N}$ can be obtained by a similar inversion applied to the PP data. We use the superscript (N) to denote effective quantities, as defined above, for N layers.

Equation (21) could be used to determine interval values of shear-wave Q, given good estimates of interval velocities and effective Q values for PP and PS modes. Thus it provides the possibility of estimating S-wave Q, using any existing surface seismic methods for Q estimation, from only PP and PS data.

Effect of the source wavelet

In order to determine actual resolution in the presence of attenuation, the initial wavelet must also be taken into account. If the wavelet is assumed to be given by the same function of time for both PP and PS wavefields, then this leads to higher resolution

for the PS case, when both wavefields are transformed to the same vertical coordinate axis, since the wavelet is compressed by the ratio V_P/V_S.

Deffenbaugh et al. (2000) considered the situation where $Q_S < Q_P$ and an initial wavelet of period ΔT_0 is assumed. For this case they predict a "crossover depth", z_c, where the resolutions are equivalent in the depth domain. The expression for crossover depth they give is:

$$z_c = \Delta T_0 Q_S Q_P \frac{V_P - V_S}{Q_P - Q_S} \tag{22}$$

Note that when $Q_S \geq Q_P$ this equation predicts infinite or negative values of z_c, which is interpreted to mean that the PS resolution always remains superior to the PP resolution at all depths. It may also be remarked that if we assume a delta function as the wavelet (for which $\Delta T_0 = 0$), the equation appears to predict crossover at zero depth. In fact, based upon the previous comparison of PP and PS Q filter responses (equations (17) and (18)), the correct interpretation is that whichever mode has the highest Q value also has the highest resolution in depth, and no crossover occurs.

MODELLED Q RESPONSES

Vertical incidence Q responses are computed using a 1-D plane-wave modelling program written in Matlab, based on equations (6)-(8). One-way constant Q attenuation for layered media is modelled for both P waves and S waves, and are then combined to compute the PP, PS and SS responses. The model used (see Table 1) is homogeneous, with events generated corresponding to a reflector at 2100m depth. There are overall differences in the amplitude levels of the impulse responses for the different modes (e.g. the amplitude ratio of impulse responses for PP and PS modes is given by $Q_P V_P / Q_{PS} V_{PS}$. For an explanation of this, see Appendix C). However, the ratio of the 2nd and 3rd event peak heights to the 1st can be seen to be independent of mode. If we consider attenuation to be a measure of how quickly amplitude decays relative to some reference depth, then this implies that the impulse responses show the same attenuation for PP, PS and SS modes. After normalizing amplitudes, impulse responses for all three modes (Figure 1) are identical in depth.

Table 1: Homogeneous model: PP, PS and SS events are modelled corresponding to unit amplitude reflection at 2100m depth.

n	Δz	V_P	V_S	Q_P	Q_S
1	2100	2100	700	50	50

The modelling is next performed starting with a 20 Hz Ricker wavelet as input (Figure 2). Time domain responses are shown in Figure 3. To better compare resolution and dispersion, the events at 2100 m depth are normalized to a peak amplitude of 1, and plotted together as a function of depth (Figure 4). The initial Ricker wavelet is identical in PP, PS and SS time, so that after conversion to depth, PS has a resolution advantage

before attenuation. In this case, where Q_S=Q_P, the advantage is retained after propagation, as seen in Figure 4(a).

It is instructive to compare these results in both temporal frequency and wavenumber domains. Figure 5 demonstrates how the PP and PS spectra arise from the combination of the initial wavelet spectrum and the Q-attenuation spectrum for the reflector at 2100 m depth (of course, Q-attenuation spectra are depth-dependent). While the wavelet spectrum is identical in both cases, the PS mode attenuation spectrum decays much more quickly as a function of frequency than PP. Compare these with Figure 6, which shows the same spectra, but now plotted as functions of PP and PS vertical wavenumbers. Now the attenuation spectrum (green curves) are seen to be identical functions of wavenumber for PP and PS, as predicted from equation (9). However, the initial wavelet spectrum is stretched in PS wavenumber relative to PP wavenumber.

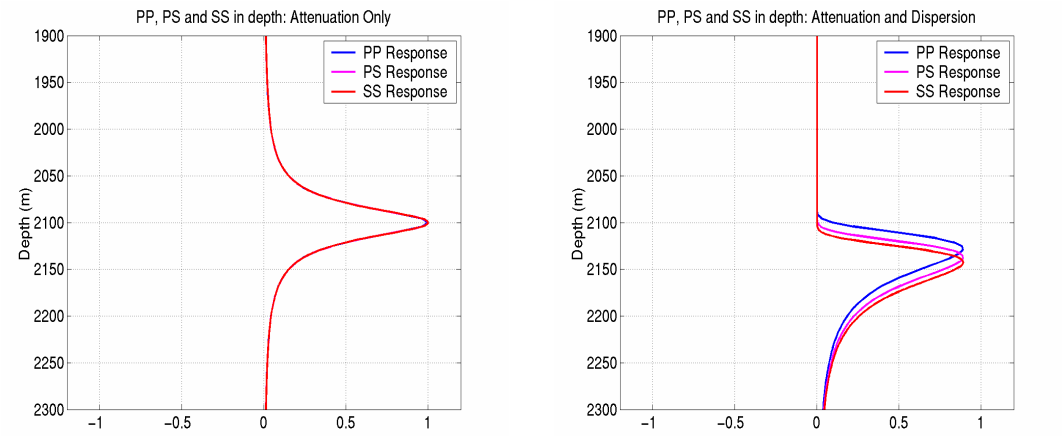

FIG 1. PP (blue), PS (magenta) and SS (red) impulse responses for the reflector at depth 2100m. The responses are displayed in depth and the Q absorption is computed: (a) using attenuation term only, giving a zero-phase response, and; (b) using both attenuation and dispersion terms, giving a minimum phase response. All of the responses have been normalized according to the maximum amplitude of the attenuation response (a) for each mode. Note that pulse shapes are identical for PP, PS and SS cases, but there are differences in onset time, due to the cut off frequency.

The modelling was performed using Q_S values 40, 30 and 20. The results for Q_S=*30* and the reflector at 2100 m depth are shown in Figure 7, plotted in depth. These should be compared with the results in Figure 4 for the Q_S=50 case. The predicted crossover behaviour occurs, such that the PS resolution appears to be similar to PP for the case Q_S =30. The period for the Ricker wavelet is computed from $T_0 = \sqrt{2}/(\pi f_{dom})$ (Sheriff and Geldart, 1995), using f_{dom} = 20 Hz, to give T_0 = 22.5ms. Inverting equation (21) to find Q_S corresponding to 2100, we get Q_S = 28.6, close to the value 30, where near equivalent resolution is observed. Thus, there appears to be good agreement with Deffenbaugh et al.'s (2000) theory. It should be noted however that: amplitude attenuation is much stronger for PS and SS than for PP, and; that the dispersion effects for PS and SS are more pronounced than for PP, as expected for the lower S-wave Q value.

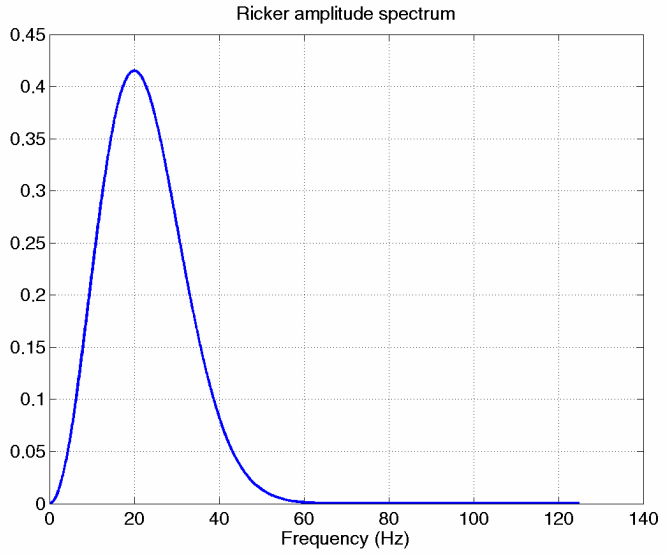

FIG. 2. Amplitude spectrum, 20 Hz Ricker wavelet used in modeling.

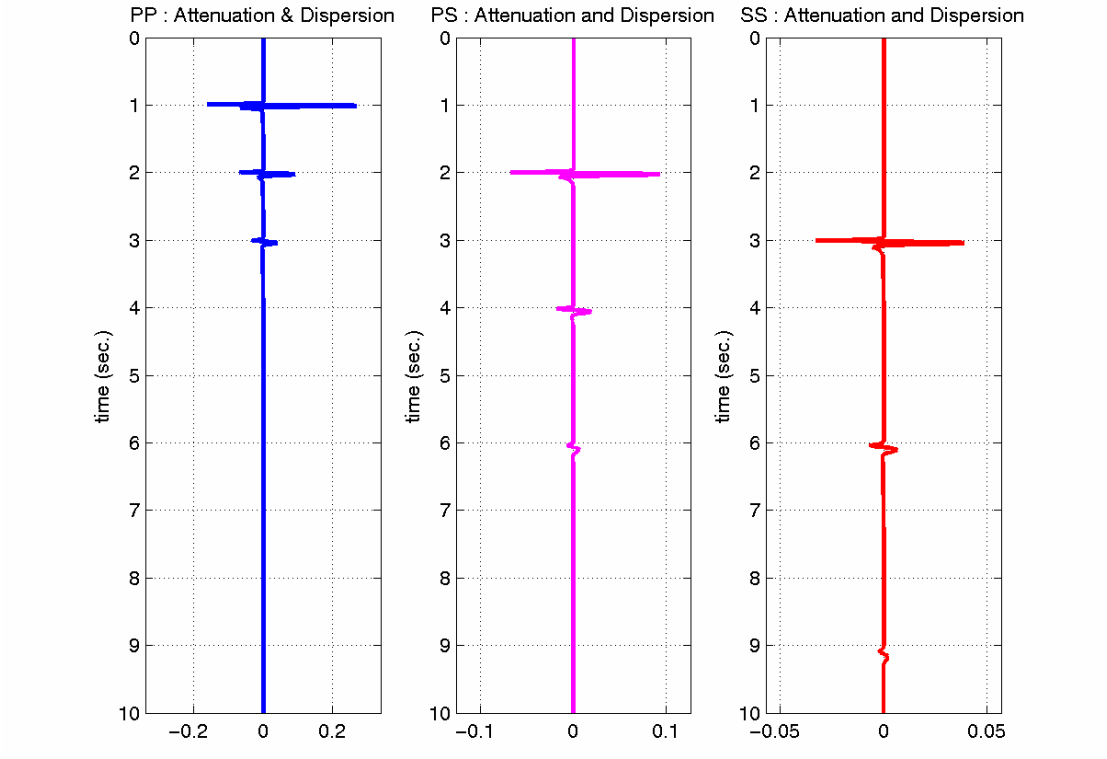

FIG. 3. Time domain seismograms for PP, PS and SS modes for model of Table 1.

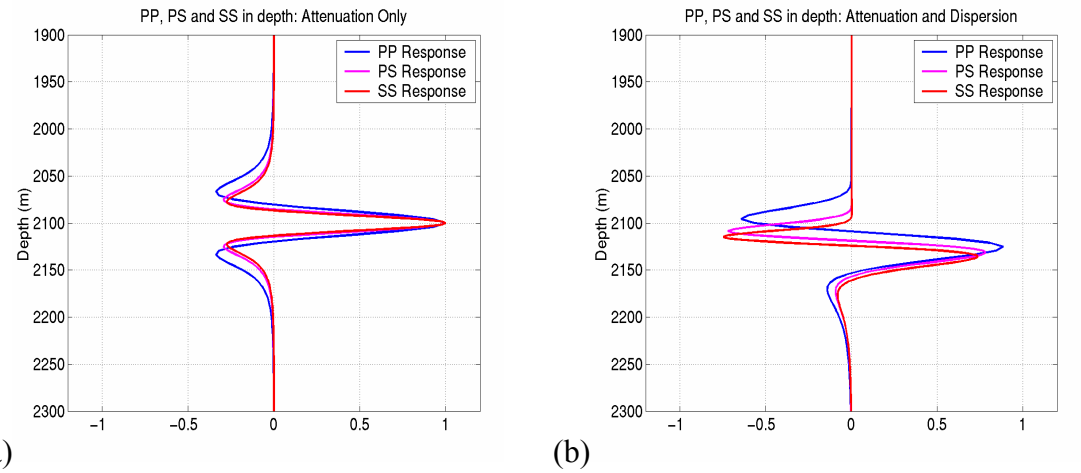

FIG 4. Depth domain seismograms for PP, PS and SS responses at 2100 metre reflector of model in Table 1. A 20 Hz Ricker wavelet is used and the Q absorption effect is computed: (a) using only the attenuation terms, and; (b) using both attenuation and dispersion terms. Note the resolution advantage of PS and SS, when Q_S=Q_P.

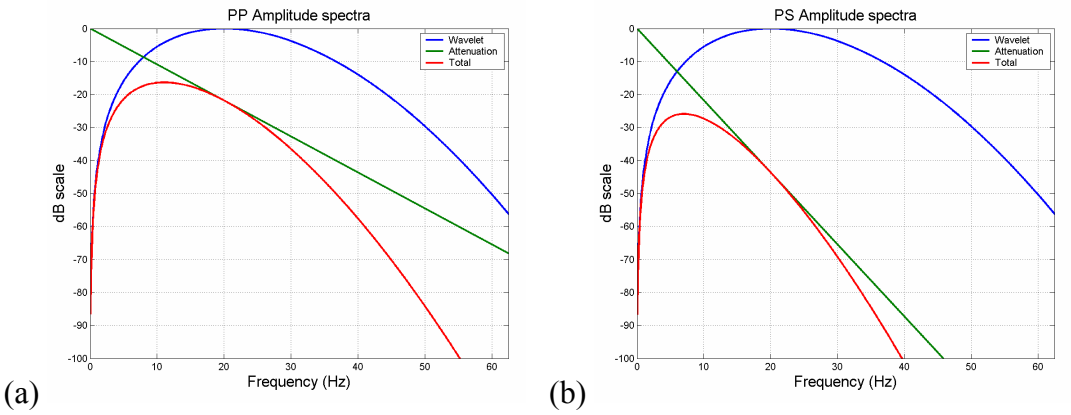

FIG 5. Temporal frequency amplitude spectra in dB for (a) PP and (b) PS event at 2100 metres depth. The blue curve is the initial Ricker wavelet spectrum, identical for both cases. The green line is the spectrum of the Q filter for that depth. The red curve shows the resulting spectrum of the pulse at depth. It is the product of the blue and green spectra. The PS event shows both an amplitude drop, and a lower peak frequency relative to PP.

Finally, we model the case of constant Q_P= Q_S but now with a very low near-surface shear velocity, using the parameters in Table 2. Reflections are generated at depths of 400 and 800 metres, though the change in velocity occurs at 500 metres depth, such that the first reflection lies entirely within the low velocity layer and the second within the high velocity layer. The model is depicted in Figure 8. The results, plotted in depth in Figure 9, show a higher resolution for the shear modes in the top low velocity layer, but the *reverse* in the deeper high velocity layer. The explanation for this effect is that, while the velocities and Q values in *all* the layers above the reflector govern the overall attenuation (by considering equations 4 and 20), the conversion to depth is based purely on the local interval velocity. The wavelet compression is much greater for a slow layer than for a fast layer, and the argument based upon wavenumbers for the homogeneous

case above no longer holds true. The wavenumber spectra for the two reflections are shown in Figures 10 and 11.

Table 2: Layered model, with low near-surface shear velocity.

N	Δz	V_P	V_S	Q_P	Q_S
1	500	1500	200	50	50
2	700	2000	1000	50	50

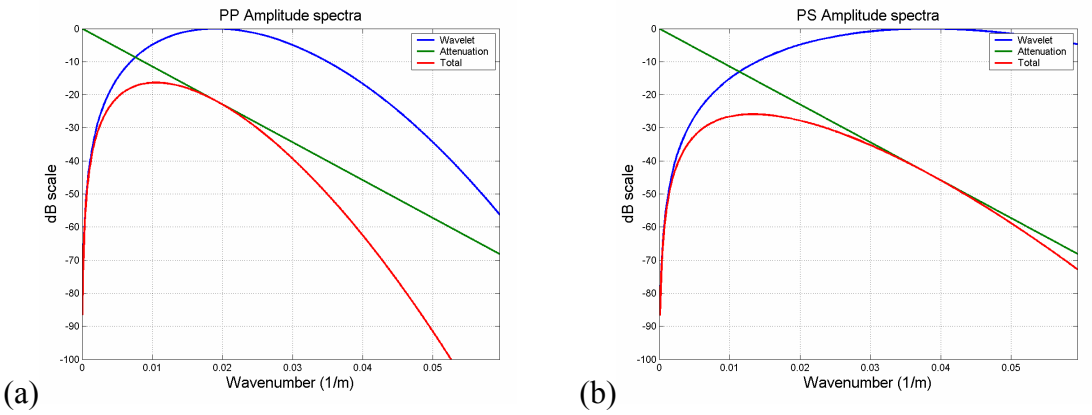

FIG 6. Vertical wavenumber amplitude spectra in dB for (a) PP and (b) PS event at 2100 metres depth. The blue curve is the initial Ricker wavelet spectrum, which has a higher wavenumber band for the PS case. The green curve is the spectrum of the Q filter, which is now seen to be invariant in wavenumber. The red curve, which is the product of the blue and green spectra, shows the resulting spectrum of the pulse at depth. The PS event is seen to have a higher peak wavenumber than PP, but lower amplitude.

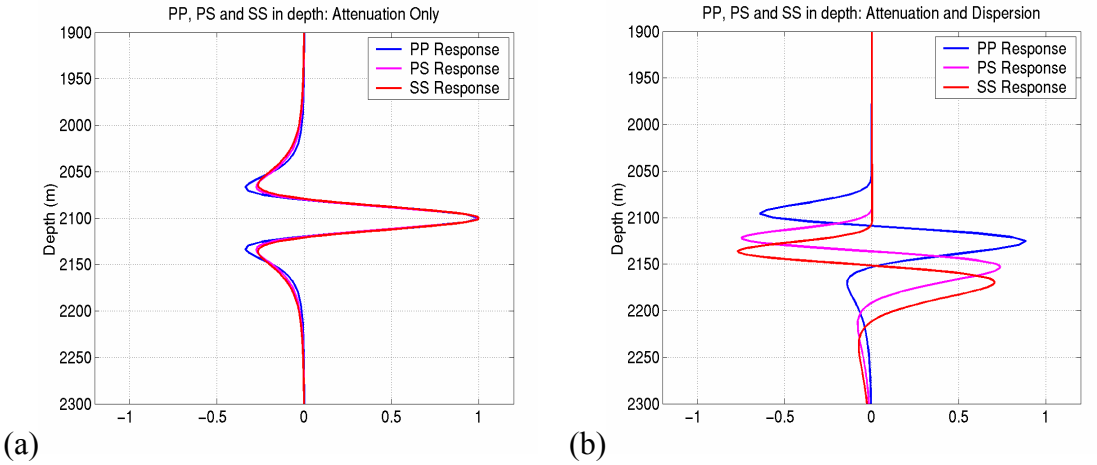

FIG 7. Depth domain seismograms for PP, PS and SS responses at 2100 metre reflector of model in Table 1, for Q_S=30, Q_P=50. The Q absorption is computed: (a) using only the attenuation terms, and; (b) using both attenuation and dispersion terms. This shows the resolution "crossover" of PP, PS and SS, for a 20Hz Ricker input. We also see significant differences in dispersion.

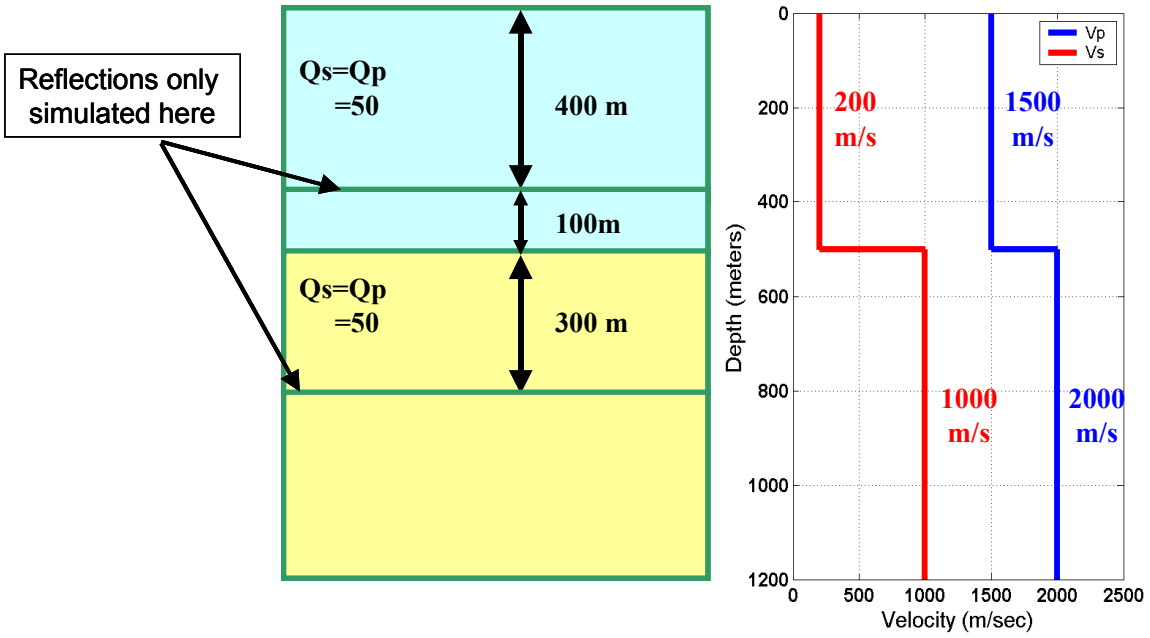

FIG 8. Velocity model for variable V_P/V_S model. Artificial reflections are generated at positions indicated.

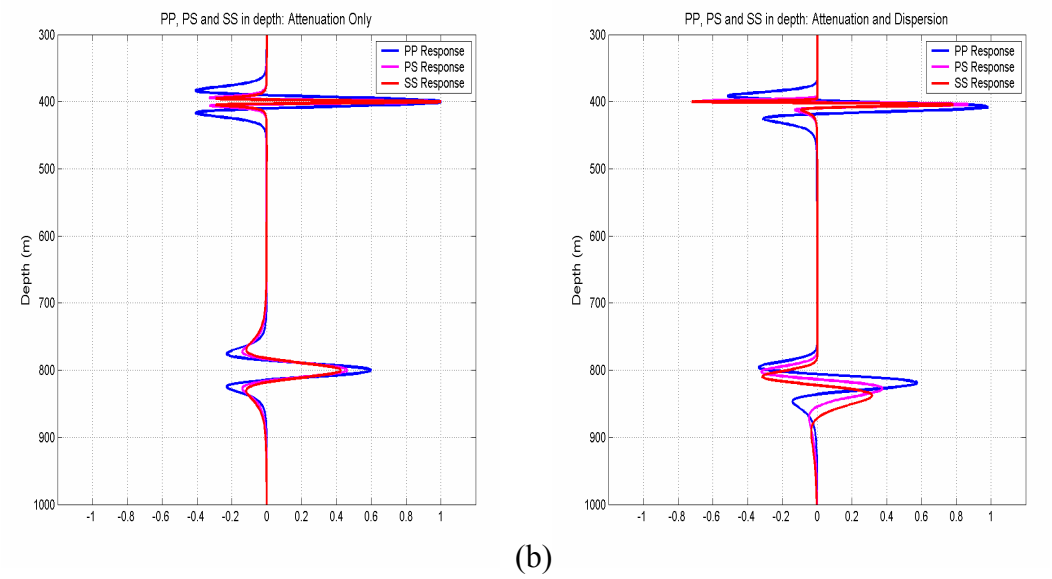

(a) (b)

FIG 9. Depth domain seismograms for PP, PS and SS responses to a 20Hz Ricker wavelet, for 500 and 800 metre reflectors of model in Table 2. The Q absorption is computed: (a) using only the attenuation terms, and; (b) using both attenuation and dispersion terms. The low velocity layer has a significant impact on S-wave resolution at depth.

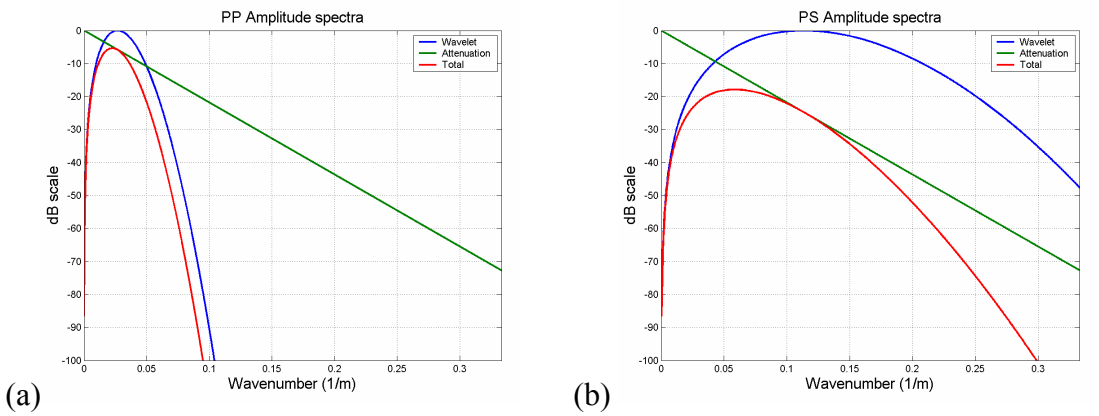

FIG 10. Vertical wavenumber amplitude spectra in dB for (a) PP and (b) PS event at 400 metres depth. As in Figure 6, the PS wavenumber spectrum benefits form the broader bandwidth of the wavelet in that domain, ensuring PS resolution remains higher than PP.

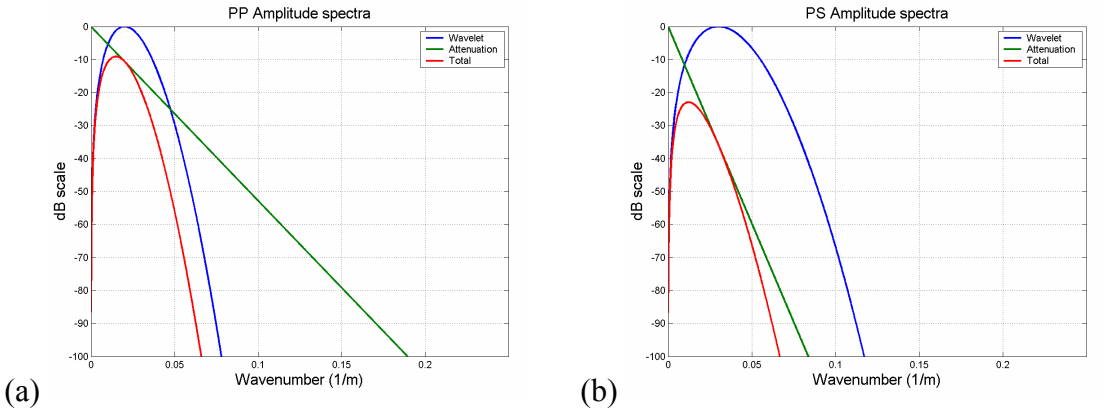

FIG 11. Vertical wavenumber amplitude spectra in dB for (a) PP and (b) PS event at 800 metres depth. The mapping between frequency and wavenumber is determined by the shear velocity in the second layer, and is no longer sufficient to compensate for the increased number of cycles in the 200 m/sec shallow shear-velocity layer. The result is that PS resolution is marginally inferior to PP resolution.

FIELD DATA EXAMPLE

Consider Figure 12, which shows a comparison of PP and PS migrated stacks from a 2-D high-resolution 3-C seismic survey at the Pikes Peak heavy oil field located east of Lloydminster, Alberta/Saskatchewan. A review of the acquisition and processing may be found in Hoffe et al. (2000).

The time axis for the PS section has been compressed by a factor of 2 relative to the PP section, which was found to approximately align corresponding events. This also enables a crude initial comparison of PP and PS resolution on the migrated data. Overall, the data quality is considered to be good. However, it is apparent that in general the PS resolution is considerably poorer than the PP resolution. For example consider the top of the Waseca formation at about 550 ms PP time (1100 PS time).

Analysis of the raw field data (Figure 13) indicates the following: the radial spectrum is deficient in low wavenumbers compared to the vertical spectrum; and the radial spectrum decays rapidly after 20 Hz, whereas the PP spectrum has a slower decay after the corresponding frequency of 40 Hz. The first effect is attributable to the initial source spectrum, which is equal in temporal frequency for both PP and PS modes, such that the low-end roll-off covers a wider range of PS wavenumbers. The second effect may well indicate a lower value of Q for shear waves than for compressional waves, or the effect of near-surface velocity ratios.

DISCUSSION AND CONCLUSIONS

The effects of Q absorption may be broadly summarized:

- Amplitude decays with propagation distance
- The seismic pulse broadens, due to differential attenuation of higher versus lower frequencies
- There is minimum-phase dispersion, consistent with the demands of causality

The intuitive argument that S-waves travelling at a slower velocity than P-waves have more oscillations and therefore more attenuation is basically correct, but can be misleading. Ultimately, we wish to compare resolution in depth rather than time, or at least compare after converting from PS to PP time. Considering the Q filter on its own, we find that the attenuation effect in depth is equal for PP and PS if they have the same Q value. However, as the source wavelet is a function of time rather than depth, it corresponds to higher wavenumbers for PS than for PP. In terms of resolution, this favours the S-waves. However, the missing low frequencies have a detrimental effect upon PS amplitudes. Figures 2 and 3 help us to understand these two effects. The resulting PS spectrum of the event has a higher peak wavenumber than PP, consistent with the observation of higher resolution in the depth domain. However, there is less overlap of the initial wavelet spectrum and attenuation spectrum, leading to overall weaker amplitudes. If the source wavelet is devoid of low-end frequencies, what remains is then subject to high absorption, diminishing the amplitude. The problem then becomes one of signal-to-noise ratio, rather than resolution.

For cases where S-wave Q is less than P-wave Q, modelling confirms the predicted crossover in resolution (Deffenbaugh et al., 2000). Furthermore, in this case the dispersion effect is stronger for PS than for PP data, which may be important to consider when matching events for V_P/V_S computation. When Q_P=50, and Q_S = 20, our modelling showed an apparent difference in depth of 50 metres, caused by dispersion. A consequence is that velocities determined from comparing PS and PP event times are likely to be affected by differences between P-wave and S-wave Q.

Perhaps the most significant finding is that a very low shear-wave velocity in the near surface may adversely affect vertical resolution at depth, even if the value of Q_S is not low. This situation may well be common. We suggest that it may be fruitful to address Q compensation of the near surface in processing to improve resolution at the reservoir.

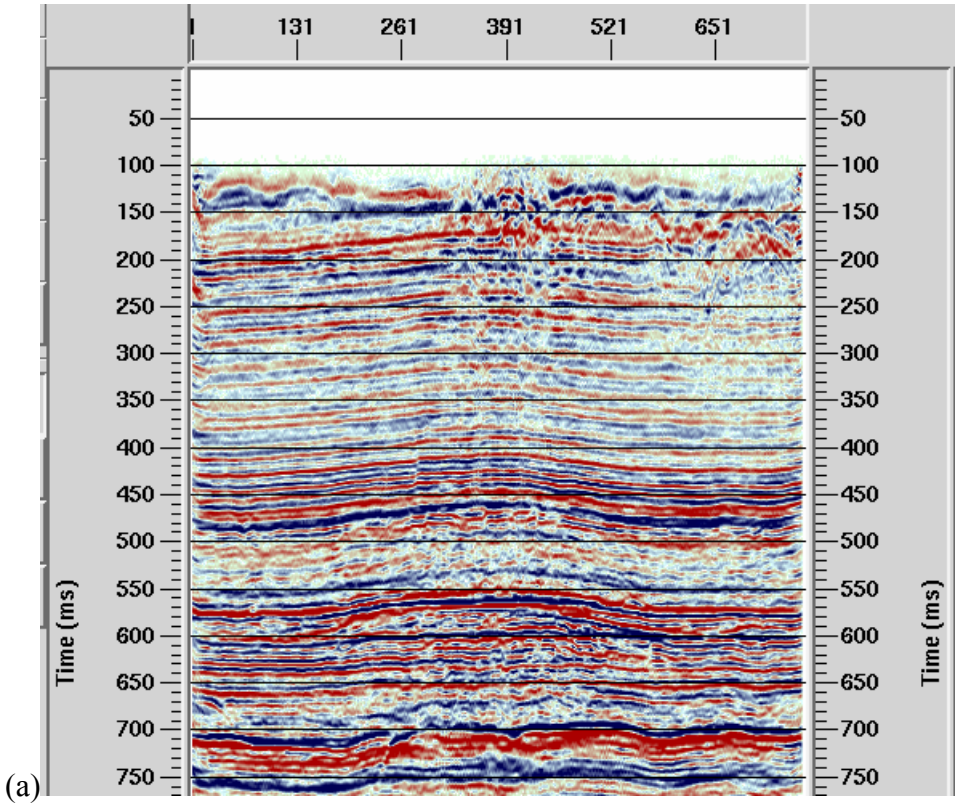

(a)

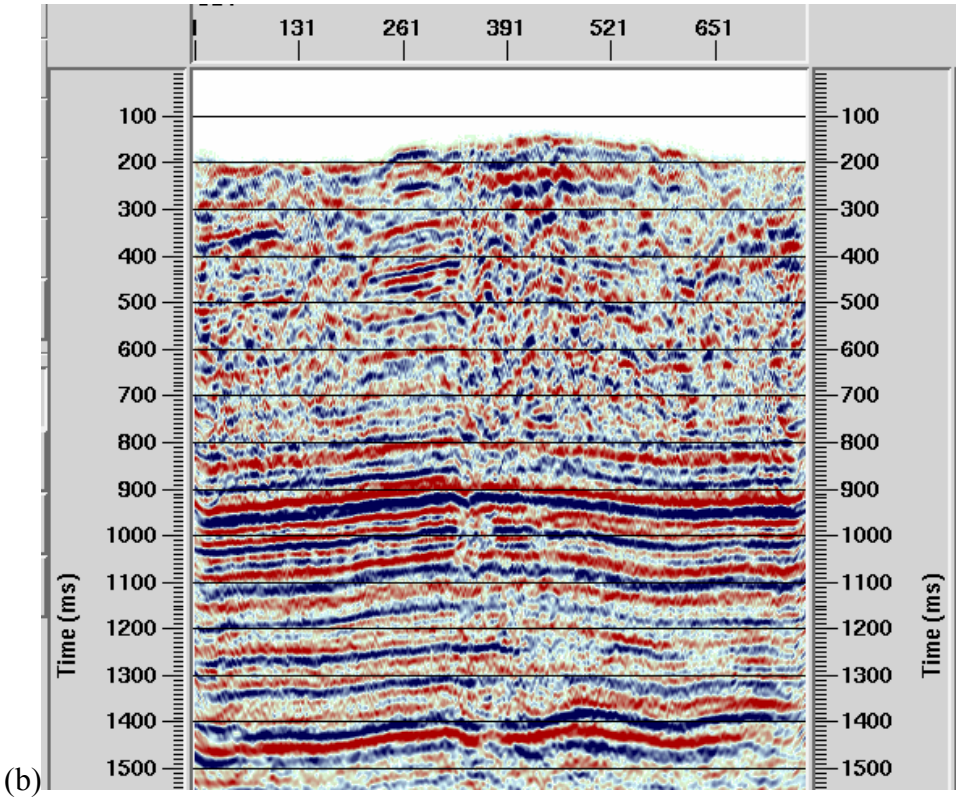

(b)

FIG 12. The Pikes Peak 3C-2D line, showing a comparison of migrated PP (a) and PS (b) stacks. The PS stack has been displayed with a compression of 2 on the time axis, which approximately aligns events with the PP section.

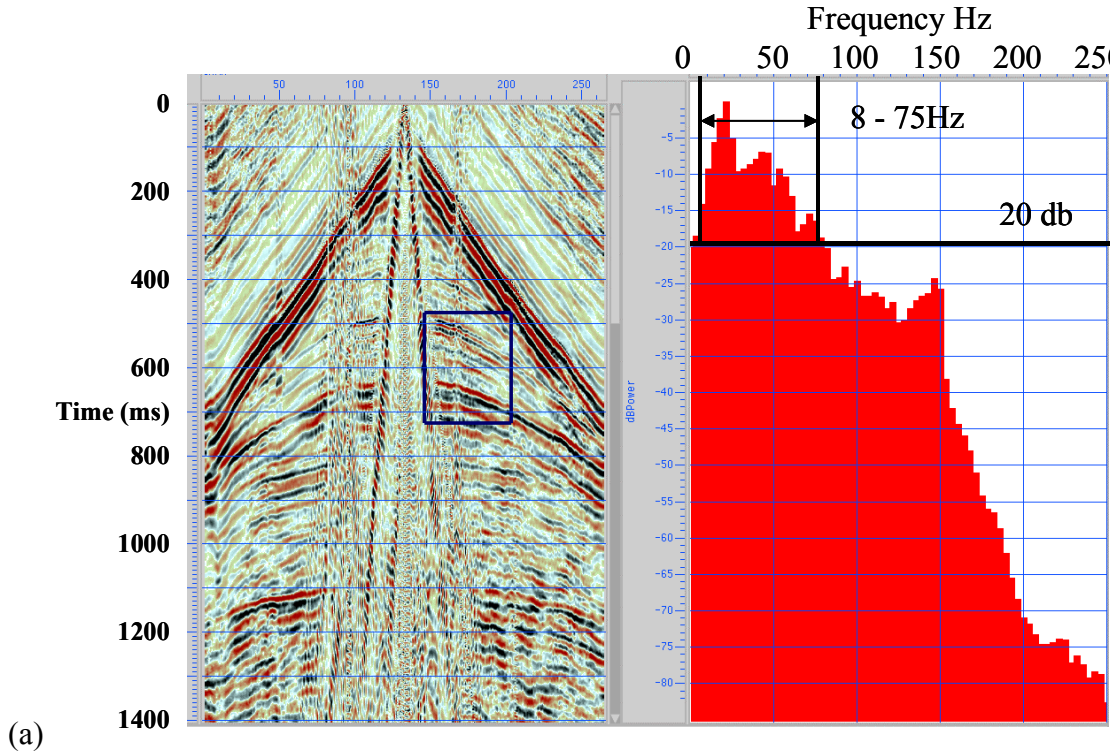

(a)

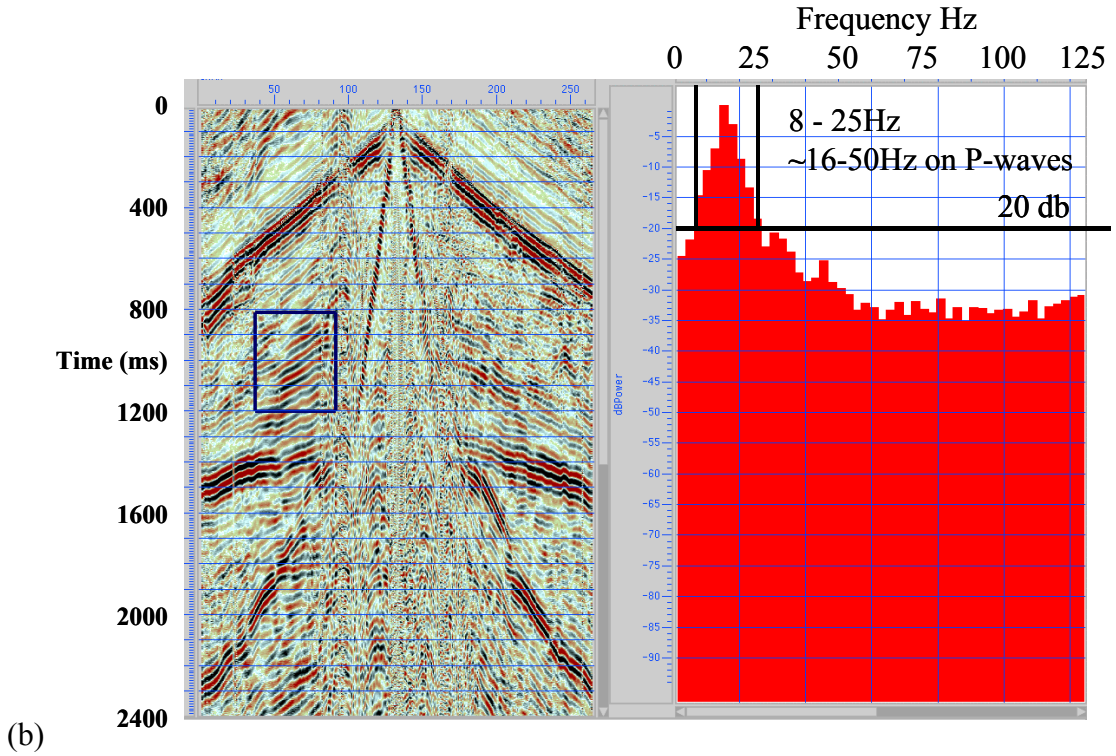

(b)

FIG 13. Comparison of prestack shot gathers for the vertical component (a) and radial component (b). The highlighted boxes indicate some P-wave and PS-wave reflection events from approximately the same depth. The bandwidth of the data in the box is shown to the right. Taking 20dB as a cut-off level, we have a signal bandwidth of 8-75Hz on the P-wave data, but only 8-25 Hz on the PS wave, corresponding to 16-50Hz after frequency axis stretch.

ACKNOWLEDGEMENTS

The authors would like to thank the CREWES sponsors for their support. We are also grateful for valuable comments by Larry Lines, Gary Margrave and Gijs Vermeer.

REFERENCES

Aki, K. and Richards, P.G., 1980, Quantitative Seismology: Theory and Methods, Vol.1: New York, W.H.Freeman and Co.

Bickel, S.H. and Natarajan, R.R., 1985, Plane-wave Q deconvolution: Geophysics, **50**, 1426-1439.

Deffenbaugh, M., Shatilo, A., Schneider B., and Zhang, M., 2000, Resolution of converted-waves in attenuating media: 70th Annual Internat. Mtg. Soc. Expl. Geoph., Expanded Abstracts, 1189-1192.

Futterman, W. I., 1962, Dispersive body waves: J. Geophys. Res., **67**, 5279–5291.

Garotta, R. and Granger, P., 2001, Some requirements of PS mode acquisition, 71st Ann. Internat. Mtg: Soc. of Expl. Geophys., 809-812.

Harrison, M.P. and Stewart, R.R., 1993, Poststack migration of P-SV seismic data: Geophysics, Soc. of Expl. Geophys., **58**, 1127-1135.

Hoffe, B.H., Bertram, M.B., Bland, H.C., Gallant, E.V., Lines, L.R., and Mewhort, L.E., 2000, Acquisition and processing of the Pikes Peak 3C-2D seismic survey: CREWES Research Report, Volume **12**.

Kjartansson, E., 1979, Constant Q-wave propagation and attenuation: J. Geophys. Res., **84**, 4737–4748.

Sheriff, R.E. and Geldart, L.P., 1995, Exploration Seismology, Second Edition: Cambridge University Press.

Udias, 1999, A., 1999, Principles of Seismology: Cambridge University Press.

Winkler, K. and Nur, A., 1979, Pore fluids and seismic attenuation in rocks, *in* Toksöz, M.N. and Johnston, D.H., Ed., Seismic wave attenuation: Soc. of Expl. Geophys., 119-122. (Reprinted from Geophysical Research Letters, v. 6, p. 1-4).

APPENDIX A

DISPERSION EQUATION FOR CONSTANT-Q ATTENUATION

Futterman (1962) used an argument based on causality to show that the attenuation and dispersion terms associated with constant-Q behaviour are related to each other through the Kramers-Kronig relations. His reasoning is too involved to repeat here, but in essence the argument used is that causality requires the complex wavenumber to be an analytic function in the upper-half complex plane. This allows use of Cauchy's residue theorem to the complex index of refraction (simply related to the wavenumber) to determine a relationship between its real and imaginary parts. The resulting Kramer-Kronig relations are given by the following Hilbert transforms (using the notation of Aki and Richards, 1980):

$$\alpha(\omega) = -\mathrm{H}\left[\omega\left(\frac{1}{c(\omega)} - \frac{1}{c_\infty}\right)\right] \tag{A1}$$

and

$$\omega\left(\frac{1}{c(\omega)} - \frac{1}{c_\infty}\right) = \mathrm{H}[\alpha(\omega)] \tag{A2}$$

where the Hilbert transform, H, with respect to ω, is given by:

$$\mathrm{H}[f(\omega)] = \frac{1}{\pi}\mathrm{P}\int_{-\infty}^{\infty}\frac{f(\zeta)}{\zeta-\omega}d\zeta$$

where $c(\omega)$ is the phase velocity, c_∞ is the limiting phase velocity at the maximum desired frequency, such that no signal can arrive at any faster velocity, $\alpha(\omega)$ is the attenuation coefficient, and P indicates taking Cauchy's principal value to remove the singularity when evaluating the integral.

APPENDIX B

LAYERED MEDIUM Q ATTENUATION

In the case of a layered medium, for vertical wave propagation, the Q filter described in equation (3) may be used recursively for each layer as follows:

$$u(z_n,t) = \frac{1}{2\pi}\int_{-\infty}^{\infty}u(z_n,\omega)e^{-i\omega t}d\omega$$

$$u(z_n,\omega) = u(z_{n-1},\omega)F_n(z_n - z_{n-1},\omega) \tag{B1}$$

$$F_n(\Delta z_n,\omega) = \exp\left(\frac{i\omega\Delta z_n}{c_n} + i\,\mathrm{H}[\alpha_n(\omega)]\Delta z_n\right)\exp(-\alpha_n(\omega)\Delta z_n)$$

where $\Delta z_n \equiv z_n - z_{n-1}$ is the thickness of layer n, c_n is the phase velocity at ω_∞ and Q_n is the Q value in layer n, and $\alpha_n(\omega) \equiv |\omega|/(2Q_n c_n)$. The recursion may be expanded to give the following for the attenuated wavefield at depth z_N:

$$\begin{aligned} u(z_N,\omega) &= u(0,\omega)\prod_{n=1}^{N}F_n(z_n,z_{n-1},\omega) \\ &= u(0,\omega)\exp\left\{i\sum_{n=1}^{N}\left(\frac{\omega}{c_n} + \mathrm{H}[\alpha_n(\omega)]\right)\Delta z_n\right\}\exp\left(-\sum_{n=1}^{N}\alpha_n(\omega)\Delta z_n\right) \end{aligned} \tag{B2}$$

Using the fact that the Hilbert transform is a linear operator to switch the order of the summation and H, we get:

$$u(z_N,\omega) = u(0,\omega)\exp\left(i\omega T + i\,\mathrm{H}\left[\sum_{n=1}^{N}\alpha_n(\omega)\Delta z_n\right]\right)\exp\left(-\sum_{n=1}^{N}\alpha_n(\omega)\Delta z_n\right) \qquad \text{(B3)}$$

where: $T = \sum_{n=1}^{N}\left(\Delta z_n / c_n\right)$

By inspection (B3) has the same form as a single-layer Q filter, where the effective Q value, Q_{eff}, is defined by:

$$\frac{T}{Q_{eff}} = \frac{2}{|\omega|}\sum_{n=1}^{N}\alpha_n(\omega)\Delta z_n \equiv \sum_{n=1}^{N}\frac{\Delta z_n}{Q_n c_n}$$

$$T \equiv \sum_{n=1}^{N}\frac{\Delta z_n}{c_n}. \qquad \text{(B4)}$$

Substitution into (B1) gives:

$$u(z_N,t) = \frac{1}{2\pi}\int_{-\infty}^{\infty} u(0,\omega)\exp\left(i\omega(T-t) + i\,\mathrm{H}\left[\frac{|\omega|T}{2Q_{eff}}\right]\right)\exp\left(-\frac{|\omega|T}{2Q_{eff}}\right)d\omega \qquad \text{(B5)}$$

where $T \equiv \sum_{n=1}^{N}\Delta z_n / c_n$ and $T/Q_{eff} = \sum_{n=1}^{N}\Delta z_n / Q_n c_n$.

An integral expression for effective Q, equivalent to (B3), is given in Bickel and Natarajan (1985), equation (33).

PS effective Q

Using a similar approach as above, based upon the P- and S-wave propagation operators for each layer gives the following equation for effective Q in the PS case:

$$\frac{T_{PS}}{Q_{PS,eff}} = \sum_{n=1}^{N}\left(\frac{\Delta z_n}{Q_{P,n}v_{P,n}} + \frac{\Delta z_n}{Q_{S,n}v_{S,n}}\right)$$

$$T_{PS} \equiv \sum_{n=1}^{N}\left(\frac{\Delta z_n}{v_{P,n}} + \frac{\Delta z_n}{v_{S,n}}\right). \qquad \text{(B6)}$$

This can also be expressed in terms of the effective Q values for P and S:

$$\frac{T_{PS}}{Q_{PS,eff}} = \frac{T_P}{Q_{P,eff}} + \frac{T_S}{Q_{S,eff}}$$

$$T_{PS} \equiv T_P + T_S, \tag{B7}$$

where T_P and T_S here are one-way P and S times. This is equation (19) in the text.

Dix-type inversion for Q_S

An inversion formula to determine the interval S-wave Q-value from the effective PS Q-values and interval P-wave Q-value can also be obtained. We use the superscript (N) to denote effective quantities, as defined above, for N layers. Using equation (B6) we get:

$$\frac{T_{PS}^{(N)}}{Q_{PS,eff}^{(N)}} - \frac{T_{PS}^{(N-1)}}{Q_{PS,eff}^{(N-1)}} = \frac{z_N}{Q_{P,N} v_{P,N}} + \frac{z_N}{Q_{S,N} v_{S,N}}. \tag{B8}$$

Rearranging, we obtain:

$$\begin{aligned} \frac{1}{Q_{S,N}} &= \frac{v_{S,N}}{z_N}\left(\frac{T_{PS}^{(N)}}{Q_{PS,eff}^{(N)}} - \frac{T_{PS}^{(N-1)}}{Q_{PS,eff}^{(N-1)}}\right) - \frac{v_{S,N}}{Q_{P,N} v_{P,N}} \\ &= \frac{1}{t_{S,N}}\left(\frac{T_{PS}^{(N)}}{Q_{PS,eff}^{(N)}} - \frac{T_{PS}^{(N-1)}}{Q_{PS,eff}^{(N-1)}}\right) - \frac{1}{Q_{P,N}\gamma} \end{aligned}, \tag{B9}$$

where $\gamma_N = v_{P,N}/v_{S,N}$ and the one-way shear interval time $t_{S,N}$ may be obtained from:

$$t_{S,N} = \frac{T_{PS}^{(N)} - T_{PS}^{(N-1)}}{1 + 1/\gamma}, \tag{B10}$$

and $Q_{P,N}$ can be obtained by a similar inversion applied to the PP data. Equation (B9) is equation (21) in the text.

APPENDIX C

SCALING RULES FOR PP-, PS- AND SS-MODE Q FILTERS

We consider only the non-dispersed form of the Q attenuation formula. For two-way propagation of P-waves to depth z, this is given by:

$$F_{PP}(z,\omega) = \exp\left(\frac{2i\omega}{V_P} z - \frac{|\omega|}{Q_P V_P} z\right).$$

The time domain pulse is given by the inverse Fourier transform:

$$f_{PP}(z,t) = \frac{1}{2\pi}\int_{-\infty}^{\infty} \exp\left(\frac{2i\omega}{V_P}z - \frac{|\omega|}{Q_P V_P}z\right) e^{-i\omega t}\, d\omega$$

$$= \frac{1}{2\pi}\int_{-\infty}^{0} \exp\left(\frac{2i\omega}{V_P}z - i\omega t + \frac{\omega}{Q_P V_P}z\right) d\omega + \frac{1}{2\pi}\int_{0}^{\infty} \exp\left(\frac{2i\omega}{V_P}z - i\omega t - \frac{\omega}{Q_P V_P}z\right) d\omega$$

$$= \frac{1}{2\pi\left(\frac{z}{Q_P V_P} + \frac{2iz}{V_P} - it\right)} + \frac{1}{2\pi\left(\frac{z}{Q_P V_P} - \frac{2iz}{V_P} + it\right)} = \frac{\frac{z}{\pi Q_P V_P}}{\left(\frac{z}{Q_P V_P}\right)^2 + \left(\frac{2z}{V_P} - t\right)^2}. \quad \text{(C1)}$$

The peak amplitude occurs when $t = 2z/V_P$, in which case we have:

$$f_{PP}(z, 2z/V_P) = \frac{Q_P V_P}{\pi z}, \quad \text{(C2)}$$

A similar analysis for PS and SS gives:

$$f_{PS}(z, 2z/V_{PS}) = \frac{Q_{PS} V_{PS}}{\pi z} \quad \text{(C3)}$$

and

$$f_{SS}(z, 2z/V_S) = \frac{Q_S V_S}{\pi z}. \quad \text{(C4)}$$

Combining these equations gives the following scaling rules:

PS over PP:

$$\frac{f_{PS}(z, 2z/V_{PS})}{f_{PP}(z, 2z/V_P)} = \frac{Q_{PS} V_{PS}}{Q_P V_P}; \quad \text{(C5)}$$

SS over PP:

$$\frac{f_{SS}(z, 2z/V_S)}{f_{PP}(z, 2z/V_P)} = \frac{Q_S V_S}{Q_P V_P}; \quad \text{(C6)}$$

where the definitions of V_{PS} and Q_{PS} are given in equation (7) .

From equations (C5) and (C6) we see that there are overall amplitude differences introduced by the Q filters for different modes, but that they are depth independent. If we regard attenuation as a measure of peak amplitude decay at depth z, relative to some reference depth z_0, then the Q-filters for different modes have the same attenuation. However, as discussed in the text, this no longer remains so when interaction with the wavelet is considered. In the case when $Q_S = Q_P$, the scaling is by the velocity ratios, or equivalently the inverse-time ratios.